Diels-Alder Reactivity of a Chiral Anthracene Template with Symmetrical and Unsymmetrical Dienophiles: A DFT Study

Jennifer P. Hernández-Mancera,[a] Francisco Núñez-Zarur,*[c] and Ricardo Vivas-Reyes*[a, b]

In this work, we used Density Functional Theory calculations to assess the factors that control the reactivity of a chiral anthracene template with three sets of dienophiles including maleic anhydrides, maleimides and acetoxy lactones in the context of Diels-Alder cycloadditions. The results obtained here (at the M06-2X/6-311++G(d,p) level of theory) suggest that the activation energies for maleic anhydrides and acetoxy lactones are dependent on the nature of the substituent in the dienophile. Among all studied substituents, only −CN reduces the energy barrier of the cycloaddition. For maleimides, the activation energies are independent of the heteroatom of the dienophile and the R group attached to it. The analysis of frontier molecular orbitals, charge transfer and the activation strain model (at the M06-2X/TZVP level based on M06-2X/6-311++G(d,p) geometries) suggest that the activation energies in maleic anhydrides are mainly controlled by the amount of charge transfer from the diene to the dienophile during cycloaddition. For maleimides, there is a dual control of interaction and strain energies on the activation energies, whereas for the acetoxy lactones the activation energies seem to be controlled by the degree of template distortion at the transition state. Finally, calculations show that considering a catalyst on the studied cycloadditions changes the reaction mechanism from concerted to stepwise and proceed with much lower activation energies.

1. Introduction

Among the chemical reactions, the Diels-Alder reaction is one of the most popular in the universe of organic chemistry. The Diels-Alder (DA) reaction represents a powerful and versatile synthetic tool to build simple and complex molecules, forming cyclic, bicyclic or tricyclic products via the formation of two new single C−C bonds.[1–5] In addition, DA is considered one of the most important reactions in organic chemistry due to its high level regio and stereoselectivity,[6–8] which usually requires electron-withdrawing groups (EWG) in the dienophile and electron-rich dienes, or *vice versa*, to afford acceptable reaction rates.[9] The mechanism of the DA reaction proceeds in a concerted way (one transition state, TS) and can be classified as synchronous or asynchronous depending on whether the new C−C bonds are or are not formed in unison.[10] However, stepwise mechanisms have been proposed for energetically favorable pathways.[11] One of the most powerful applications of DA reactions is the possibility of obtaining biologically active compounds for several applications. For instance, chiral anthracene derivatives have attracted attention because their cycloaddition with appropriate achiral dienophiles[6] give access to butenolides, α,β-unsaturated, γ-lactams and related compounds with high stereocontrol, regiospecificity and diastereoselectivity, by using the concept of asymmetric induction to obtain enantiomerically pure substances. These types of compounds have interesting biological properties, such as the central role in the inhibition and control of pathogenic bacteria with biofilm forming activity,[12] among other biological qualities and applications.

Anthracene templates have been used since the mid-50s as stereocontrolling agents in DA and retro-DA reactions with dienophiles based on maleic anhydride and maleimide skeletons (Scheme 1).[6,7,13–19] For instance, Snyder and co-workers studied the DA cycloadditions of several chiral (9-anthryl) carbinol templates ($R_1 = -CH_3$, $-CF_3$; $R_2 = -H$, *n*-butyl, Ac, $-CH_3$; $R_3 = -H$) with a series of symmetrical and nonsymmetrical dienophiles based on maleic anhydride and maleimides ($X = O$, NH, NMe; $R_4 = -H$, $-Br$, $-CH_3$, $R_5 = =O$) with a good facial selectivity and regioselectivity under thermal and Lewis catalyzed conditions.[7] A few years later the same authors used Pirkle's alcohol (anthracene template with $R_1 = -CF_3$; $R_2 = -CH_3$; $R_3 = -H$) for DA cycloaddition with 5-acetoxyfuranone ($R_4 = -H$, $R_5 = -CO_2CH_3$) with very low conversion.[6] However, the
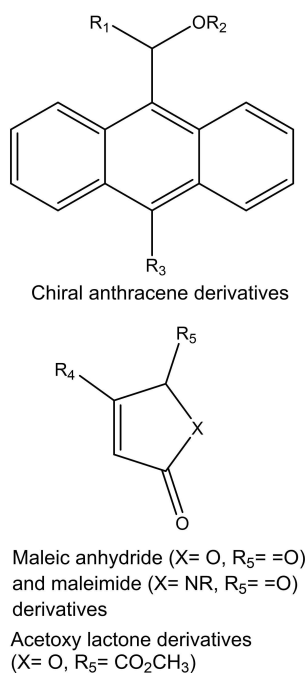
[a] *J. P. Hernández-Mancera, Prof. R. Vivas-Reyes*
Grupo de Química Cuántica y Teórica
Facultad de Ciencias Exactas y Naturales
Universidad de Cartagena
Campus San Pablo
Cartagena 130015 (Colombia)
E-mail: rvivasr@unicartagena.edu.co

[b] *Prof. R. Vivas-Reyes*
Grupo CipTec, Fundación Universitaria
Tecnológico de Comfenalco
Facultad de Ingenierías
Cartagena de Indias
Bolívar 130001 (Colombia)

[c] *Prof. F. Núñez-Zarur*
Facultad de Ciencias Básicas
Universidad de Medellín
Carrera 87 N° 30–65
050026 Medellín (Colombia)
E-Mil:
E-mail: fnunez@udem.edu.co

ChemistryOpen

Full Papers
doi.org/10.1002/open.202000137

Chemistry Europe
European Chemical
Societies Publishing

Scheme 1. Chiral anthracene templates and dienophiles used for DA cyclo-additions.
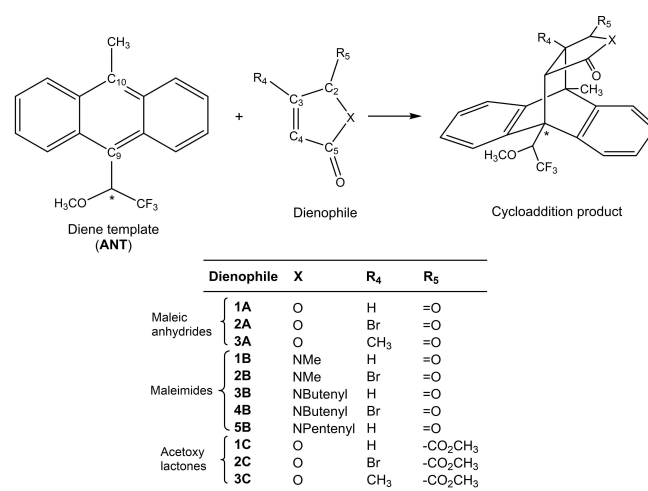
analyzing the energetics and the topology of the transition states for the cycloadditions.

While these studies provided very useful information about the reaction mechanism of DA reactions using chiral anthra-cenes, they are limited to one type of dienophile and an anthracene template with substitution only at C9 (that is, $R_3 = -H$ in Scheme 1) and they do not explore the effect of substituents on the structures and energetics of the cyclo-additions. Moreover, the detailed electronic characterization of these reactions has not been provided. In this contribution, we use computational chemistry based on DFT calculations to explore the effect of dienophile substituents in a series of eleven dienophiles including substituted maleic anhydrides, maleimides and acetoxy lactones and the chiral anthracene template 10-methyl-9-(1-methoxy-2,2,2-trifluoroethyl)-anthracene. Specifically, our goal is to provide a detailed molecular picture of the DA reactions mentioned above by looking at the energetics of the reactions, charge transfer (CT) effects, and frontier molecular orbitals (FMO). Furthermore, the application of the Activation Strain Model (hereafter ASM)[22,23] may help us to understand the origin of the calculated activation energies. Finally, we provide a rationale on the effects of Brønsted catalysts on the reaction mechanism.

Computational Details

The DA reaction between 10-methyl-9-(1-methoxy-2,2,2-trifluor-oethyl) anthracene (hereafter **ANT**) and eleven dienophiles is shown in Scheme 2.

The anthracene template used as a model diene was synthesized by Snyder and co-workers,[6] which bears a chiral substituent at C9 ($C(CF_3)(H)(OCH_3)$) and a methyl group at C10. This template has not been studied previously using computational methods and there-fore the effect of the methyl group at C10 has not been explored. The eleven dienophiles bear different heteroatoms (O, N-methyl, N-butenyl, N-pentenyl) and substituents at R_4 ($-H$, $-Br$, $-CH_3$) and R_5 positions ($=O$, OAc) and were selected to cover a wide range of

inclusion of an electron donor group (EDG) at R_3 ($-CH_3$) led to 10-methyl-9-(1-methoxy-2,2,2-trifluoroethyl)anthracene, a tem-plate which proved to be stable against oxygen and much more reactive than the previous one, giving the cycloaddition product with maleic anhydride ($X=O$; $R_4=-H$, $R_5==O$) with about 95% yield and almost complete diastereoselectivity.[6] Later on, (−)-(R)-9-(1,2-dimethoxyethyl)anthracene ($R_1 = -CH_2OCH_3$; $R_2=-CH_3$; $R_3=-H$) was used as a chiral template for DA cycloadditions with maleimides and maleic anhydrides for the synthesis of α,β-unsaturated γ-lactams.[13]

Other contributions from the group of Jones focused on the combination of experimental and computational techniques based on Density Functional Theory (DFT) calculations calcu-lations for the exploration of the effect of the electronic nature and size of maleimide substrates ($X=NR$, variety of R groups; $R_4=-H$) in the cycloaddition with 9-(1-hydroxyethyl)-anthracene ($R_1=-CH_3$; $R_2=-H$; $R_3=-H$) and 9-(1-meth-oxyethyl)-anthracene ($R_1=-CH_3$; $R_2=-CH_3$; $R_3=-H$)[14] and more recently to study the effect of hydrogen bonds in the selectivity of several 9-(2-aminoethyl)anthracene derivatives in reactions with N-methyl maleimides.[15]

All these studies demonstrated that chiral control in DA reactions is significant for obtaining molecules with attractive applications. In order to achieve more insightful information at molecular level, several contributions have been devoted to the computational study of the DA cycloaddition between chiral anthracenes and dienophiles with a variety of substituents using DFT calculations. The most relevant contributions to the topic come from the group led by Aviyente, which has studied the diastereoselectivity of DA reactions[20] and the effect of the hydrogen bond control in the reaction output[21] by closely

Dienophile		X	R_4	R_5
Maleic anhydrides	**1A**	O	H	=O
	2A	O	Br	=O
	3A	O	CH_3	=O
Maleimides	**1B**	NMe	H	=O
	2B	NMe	Br	=O
	3B	NButenyl	H	=O
	4B	NButenyl	Br	=O
	5B	NPentenyl	H	=O
Acetoxy lactones	**1C**	O	H	$-CO_2CH_3$
	2C	O	Br	$-CO_2CH_3$
	3C	O	CH_3	$-CO_2CH_3$

Scheme 2. Cycloaddition reactions studied in this work between a chiral anthracene template **ANT** and eleven dienophiles **1 A** to **3 C**. The chiral group in the template is labelled with *. The numbering of the most important atoms in the template and dienophiles is shown.

ChemistryOpen

Full Papers
doi.org/10.1002/open.202000137

Chemistry Europe
European Chemical
Societies Publishing

dienophile architectures used in different experimental studies from Snyder and Jones,[7,14] including maleic anhydrides, maleimides and acetoxy lactones. To the best of our knowledge, no computational studies on the effect of these reactants in DA reaction mechanism has been reported until now. It is worth mentioning at this point that only the *endo* product was considered as the main product (Scheme 2) due to its high diastereo- and regioselectivity yield (95%) in the cycloaddition.[6] However, in order to be exhaustive, we also performed few calculations of the reaction mechanisms leading to the *exo* product (*vide infra*).

Gas phase calculations were performed to localize all stationary points (minima and transition states) in the potential energy surfaces (PES) by means of Density Functional Theory (DFT) calculations as implemented in the Gaussian 09 program.[24] For geometries and energetics the hybrid meta-GGA M06-2X exchange correlation functional[25] was used in combination with the 6-311 + +G(d,p) basis set.[26] The M06-2X exchange correlation functional was chosen due to its performance to predict the thermodynamics and kinetics of the Diels-Alder reactions, which properly describes non-covalent interactions necessary for the adequate description of transition states and adducts.[27,28] All reactions were followed along the intrinsic reaction coordinate (IRC) and all minima and transition state structures were verified by harmonic frequency calculations.[29]

All wavefunction analyses at minima and transition state structures were performed using the M06-2X functional and the TZVP basis set of Ahlrichs and co-workers[30] based on the M06-2X/6-311 + +G(d,p) optimized geometries. These calculations include atomic charges and charge transfer, which were obtained from Natural Population Analysis (NPA) of the natural bond orbital (NBO)[31,32] analysis. The charge transfer between fragments at the transition states was calculated as the summation of NPA derived partial atomic charges of every atom of the dienophile moiety. FMO and energy gaps were also computed for separate reactants, the reactive complexes (RC, *vide infra*) and transition states using Kohn-Sham orbitals. Calculations of orbital overlap (S) at the transition states was achieved through a fragment-based approach using the Multiwfn v3.7 software[33] according to the equation 1:

$$S_{ij} = \int \varphi_i^{diene}(\boldsymbol{r})\varphi_j^{dienophile}(\boldsymbol{r})d\boldsymbol{r} \qquad (1)$$

where i and j are the indexes of the molecular orbitals of interest and ϕ is the fragment wavefunction at the geometry of the transition state.

The Activation Strain Model was also applied to the reactions studied here in order to gain more insights into the possible origin of the calculated activation energies. In this model, the activation energy $\Delta E^{\ddagger}$ is decomposed into two main contributions: the activation distortion or activation strain energy $\Delta E^{\ddagger}_{strain}$ and the activation interaction energy $\Delta E^{\ddagger}_{int}$, according to equation 2:

$$\Delta E^{\ddagger} = \Delta E^{\ddagger}_{strain} + \Delta E^{\ddagger}_{int} \qquad (2)$$

The $\Delta E^{\ddagger}_{strain}$ term in equation 2 is a destabilizing term (always positive) and indicates how much the reactants structurally deform themselves to achieve the geometry of the transition state. This term can be further decomposed into two terms corresponding to the strain energy of each one of the fragments. The $\Delta E^{\ddagger}_{int}$ term refers to the electronic structure of the fragments and how they orient to get the proper geometry of the transition state. These calculations were performed at the M06-2X/TZVP level based on M06-2X/6-311 + +G(d,p) optimized geometries with Gaussian 09. The interaction energy ΔE_{int} may also be further decompose into

several terms using the Energy Decomposition Analysis (EDA) method originally proposed by Morokuma, Ziegler and Rauk.[34–36] In this case,

$$\Delta E_{int} = \Delta E_{elect} + \Delta E_{Pauli} + \Delta E_{orb} = \Delta E_{steric} + \Delta E_{orb} \qquad (3)$$

where ΔE_{elect} quantifies the classical electrostatic interactions between deformed reactants (usually attractive if the two fragments are neutral), ΔE_{Pauli} corresponds to the Pauli exchange repulsion between fragment occupied orbitals (always destabilizing) and ΔE_{orb} comprises the interaction between occupied and unoccupied fragment orbitals accounting for charge transfer, HOMO-LUMO interactions and polarization effects. The first two terms may be combined into a single one, which is called the steric-repulsion term ΔE_{steric}. The EDA method was applied to each one of the transition states calculated here to allow the quantification of the ΔE_{steric} and ΔE_{orb} terms of the interaction energy at the M06-2X/TZVP level using the Multiwfn software,[33] which perform a simple EDA based on a fragment approach by combining the fragment wavefunctions into an initial guess for the complex molecule.

Since the diene template is invariant in all calculations (**ANT**), the nomenclature adopted in this work for the different intermediates and transition state structures will be constructed from a prefix ("**RC**" for a reactant complex, "**TS**" for a transition state, "**P**" for a product) followed by the label of the corresponding dienophile, as shown in Scheme 2.

2. Results and Discussion

In this work, we have studied the DA reaction between a chiral anthracene template (**ANT**) and a series of eleven dienophiles with different substitution patterns. However, we must note that **ANT** bears a chiral group at C9 (see Scheme 2). As a consequence, different conformations are possible resulting from rotation of the $C(CF_3)(H)(OCH_3)$ substituent along the C9–C10 axis. In order to obtain a minimum energy structure of the template, we scanned the dihedral angle around the C9–C* bond. Three main conformers were detected, which are shown in Figure S1 of the Supporting Information. The lowest energy structure (conformer **C**) has the trifluoromethyl group located in a perpendicular disposition with respect to the plane of the anthracene core, whereas other conformers are higher in energy by 4 and 20 kcal mol^{-1}. In view of these results, we selected conformer **C** as the true minima for all subsequent calculations.

Another key feature of the anthracene template used here is the presence of the methyl substituent at C10 (Scheme 2). Experiments from the Snyder group[6] revealed that the DA cycloaddition of a chiral template with no substituents at C10 with dienophile **1 C** led to an *endo* product with only 16% yield. When including a methyl group at C10 the yield of the reaction increased to 88%, although it resulted in a 6:1 mixture of regioisomers (*endo*: *exo*) from the two different approaches of the dienophile. Test calculations were performed in order to confirm the effect of the methyl group in **ANT** on the DA reactivity. The results (Figure S2 and Table S1 of the Supporting information) suggest that the presence of the methyl substituent led to a less exergonic reaction accompanied by a lower

ChemistryOpen

Full Papers
doi.org/10.1002/open.202000137

Chemistry Europe
European Chemical
Societies Publishing

energy transition state of cycloaddition, leading to a lower activation energy.

2.1. Diels-Alder Cycloadditions Between ANT and Dienophiles 1 A–3 C

We analyzed in detail the reaction between **ANT** and the eleven dienophiles **1 A–3 C** considered in this work (Scheme 2). A sketch of the PES for the DA cycloadditions explored here are shown in Figure 1. All reactions show the presence of an energy minima formed from separate reactants that evolve to the transition state structure. This minima can be regarded as a reactant complex (RC) where both diene and dienophile fragments are weakly bound. The optimized structures of all reactants and RCs are shown in Figures S3 and S4 of the Supporting Information and the transition state structures are shown in Figure 2.

The mechanism explored in this contribution is based on experimental evidence which[7,13] shows that chiral anthracenes lead mainly to the *endo* product (>70% yield) during cycloaddition with a variety of dienophiles. Therefore, this study will focus on the mechanism leading to the *endo* product. However, in order to be exhaustive, the mechanism leading to the *exo* product was also considered for a few dienophiles (unsubstituted at R_4). The outcomes (Figure S5 and Table S2 of the Supporting Information) indicate that the formation of the *exo* products are less exergonic and the associated activation energies are between 5.1 and 8.3 kcal mol^{-1} higher than those of the *endo* one. Thus, the consideration of the *endo* mechanism for all reactions here is fully justified.

A critical feature of the DA reactions studied here is the presence of hydrogen bond interactions in both the RC and TS structures (Figures 2 and S4). Such intermolecular hydrogen bonds have been suggested to be the origin of the diastereoselectivity in reactions involving chiral dienes, and this topic has already been assessed using computational chemistry.[15,21] Therefore, we shall not focus on the role of hydrogen bonding in the studied DA reactions, but rather on the reactivity trends and electronic properties that characterize such cycloadditions.

Following the profile in Figure 1, when the anthracene and the dienophile approach each other a RC is formed prior to the transition state. This is in agreement with previous computational studies of similar reactions where molecular complexes have been found on the potential energy surface of DA cycloadditions.[37–40] The formation of RCs as intermediates in DA cycloadditions has been a topic of debate since the mid-50s.[16,37,40–49] For instance, the formation of a molecular complex in the DA reaction between anthracene and maleic anhydride was proposed by Andrews and Keefer.[16] However, only in 1975 Kiselev and Miller successfully proved that the reactant complex is a true intermediate in the DA cycloaddition between 9,10-dimethyl anthracene and tetracyanoethylene (TCNE).[42] Nevertheless, the true identity of this molecular complex as an CT intermediate or a nonreactive side equilibrium complex remained elusive for years and several authors did their own contributions to the topic with frequently opposed
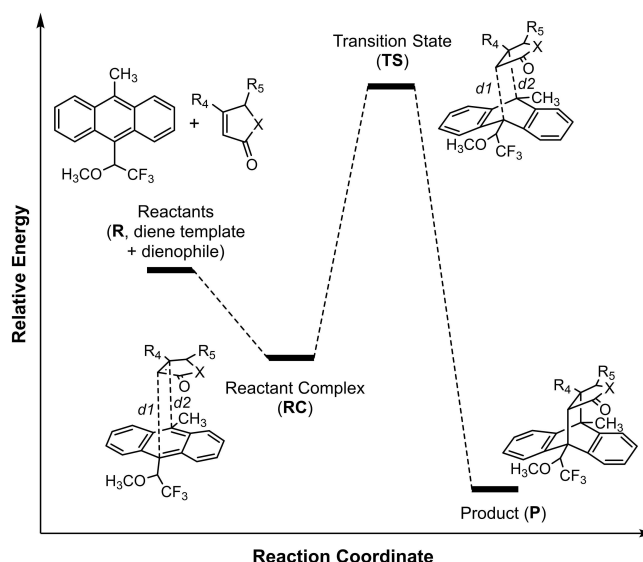

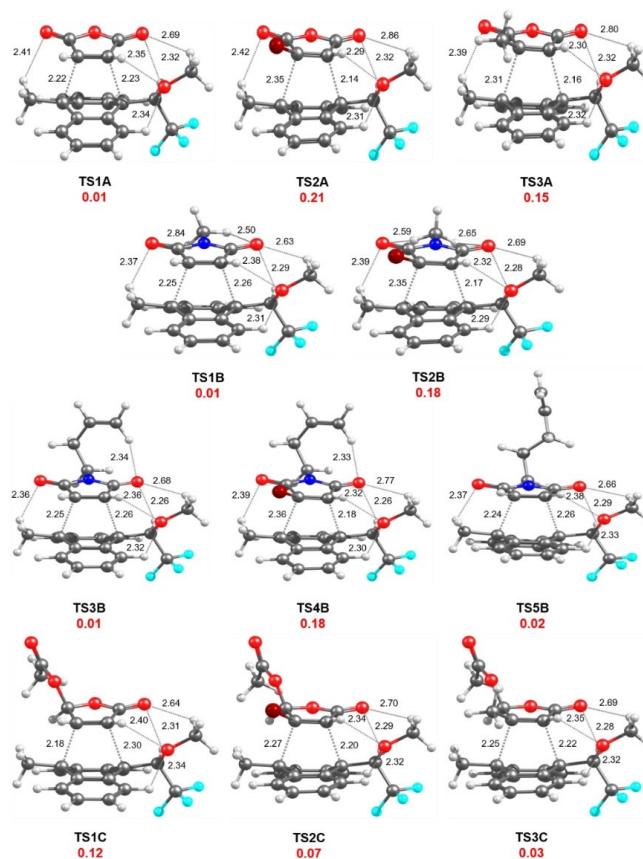**Figure 1.** Qualitative potential energy profile for the DA cycloadditions studied in this work

Figure 2. Transition state structures for the reaction of **ANT** with dienophiles **1 A–3 C** obtained at the M06-2X/6-311++G(d,p) level of theory. The bond lengths and hydrogen bond interactions are reported in angstroms (Å). The synchronicity ($\Delta d = |d1-d2|$) of the TS is reported in red.

conclusions.[37,42,44,46,47] With the advance of computational methods in the past two decades, computational chemistry also played a role by discriminating the proper mechanism of DA

ChemistryOpen

Full Papers
doi.org/10.1002/open.202000137

Chemistry
Europe
European Chemical
Societies Publishing

cycloadditions. Accordingly, theoretical calculations seemed to indicate that a CT complex is indeed an intermediate during the reaction of anthracene and TCNE.[37] Few years later an X-ray structure of a CT complex during cycloaddition of anthracene and of 4-nitrobenzodifuroxan (NBDF) was obtained, although according to the authors this complex does not seem to resemble the geometry of the transition state.[46] Here, we found RC intermediates similar to that reported by Wise and Wheeler[37] and Howard *et. al.*[40] In our case, all obtained RCs share similar geometrical features with only small variations resulting from the different substitution patterns in the dienophile (Figure S4). In these intermediates the *d1* distances range from 3.02 to 3.10 Å while *d2* distances have values between 3.10 and 3.33 Å, indicating a weak interaction between fragments. The largest values of *d1* and *d2* distances correspond to the acetoxy lactone systems, as a result of the significant steric repulsion between the carbon atom bearing the OAc substituent, which is a sp^3 carbon, and the anthracene ring. The relatively large intra-fragment distances in the RCs do not significantly modify the planarity of both ring systems and they appear to preserve their geometrical features when compared to the isolated molecules. This is further corroborated by the ASM calculations (*vide infra*).

Afterwards, the TS that connects the RC and the product (P) appears. As in the case of the RCs, all TS structures located here share similar geometrical features (see Figure 2). In this case, both rings lose their planarity as a result of strong orbital interactions between the π systems of both ring systems. For the anthracene template, for instance, a significant pyramidalization about the C9 and C10 carbon atoms is observed. In general, the loss of planarity is smaller for the dienophile moiety compared to the anthracene core, an effect which is also corroborated by the ASM calculations (*vide infra*). The *d1* and *d2* distances in the TS structures vary from 2.14 to 2.30 Å (*d1*) and 2.18 to 2.36 Å (*d2*). Regarding these intra-fragment distances at the TS, we may look at the degree of synchronicity. The synchronicity/asynchronicity has been geometrically tackled from the absolute difference between the incipient C–C single bonds length ($\Delta d = |d1-d2|$)[27,50] in the TS geometries (see Figure 2). We must note here that several authors[25,27,51] have suggested that the M06-2X exchange correlation functional reliably predicts energy, geometry and the degree of asynchronicity in the formation of new C–C single bonds in DA reactions. Consequently, we must expect that our methodology provides good estimates of the TS geometries even when kinetic data for the studied reactions are not available and, hence, the methodology calibration is not possible.

Taking as reference the TS structure between an anthracene template without substituents and dienophile **1 A** (Figure S6 in the Supporting Information), which is a perfectly synchronous transition state ($\Delta d = 0$), we can observe the variation of the distances when adding substituents in such a way that when Δd values are close to zero it is considered to be a synchronous concerted mechanism.[50] In general, highly synchronous TS structures ($\Delta d < 0.03$ Å) are obtained only for dienophiles with no substituents at R4 (**TS1A**, **TS1B**, **TS3B** and **TS5B**). When substituents at R4 are introduced, the synchronicity of the DA

cycloaddition is lost, and asynchronous TS structures are observed. A clear exception to this trend is the group of acetoxy lactones, for which the TS structures **TS1C** and **TS2C** are asynchronous ($\Delta d = 0.12$ and 0.07 Å) while **TS3C** is synchronic ($\Delta d = 0.03$ Å).

Turning out to the energetics, Table 1 shows the Gibbs energies in gas phase at 25 °C for all stationary points of the DA reactions of the eleven dienophiles **1 A–3 C** (all normalized with respect to the system *ANT + dienophile*). The corresponding electronic energies are displayed in Table S3 of the Supporting Information. Calculations show that all studied DA cycloadditions are favorable as evidenced by the highly exergonic reaction energies of the process **R→P** (ΔG_{298} between −24.1 and −13.0 kcal mol^{-1}). When looking at the relationship between reaction energies and the activation energies (Figure S7 of the Supporting Information) we found very good linear correlations, indicating a Bell-Evans-Polanyi relationship for all studied dienophiles.[52]

As observed from Table 1, formation of RCs is favorable in all cases with energies ranging from −4.5 (dienophile **2 B**) to −1.1 kcal mol^{-1} (dienophile **1 C**), indicating that the diene and dienophile fragments in these complexes are held together by weak interactions. The energies of the transition states range from 13.2 (dienophile **1 B**) to 24.4 kcal mol^{-1} (dienophile **3 C**). For the three groups of dienophiles (see Scheme 2), we will discuss the trends in activation energies for maleic anhydrides (**TS1A**, **TS2A**, **TS3A**), maleimides (**TS1B**, **TS2B**, **TS3B**, **TS4B**, **TS5B**) and acetoxy lactones (**TS1C**, **TS2C**, **TS3C**) separately. At this point it is worth to note that the activation energies discussed in this work will be taken as the energy of the corresponding TS structures. In general, within the three sets of dienophiles the lower energy barriers are observed for those reactions with unsubstituted dienophiles (R$_4$=−H). For maleic anhydrides, the lowest energy transition state corresponds to **TS1A** ($\Delta G^{\ddagger}_{298} = 14.9$ kcal mol^{-1}) while dienophiles **2 A** and **3 A** show TS structures that are 1.6 and 4.0 kcal mol^{-1} higher in energy, respectively. These results indicate that substitution at R$_4$

Table 1. Gibbs energies (in kcal mol^{-1}) at 25 °C of all stationary points located along the PES for the reaction between **ANT** and dienophiles **1 A–3 C** (see Scheme 2 for labelling of the dienophiles) obtained at the M06-2X/6-311++G(*d,p*) level of theory. The stationary points of the reactions involving maleic anhydrides bearing −F, −Cl and −CN substituents at R$_4$ are also included. All energies have been normalized to the system *ANT +dienophile*.

Dienophile	R	RC	TS	P
1 A	0.0	−2.9	14.9	−20.9
2 A	0.0	−3.3	16.5	−20.4
3 A	0.0	−3.7	18.9	−15.5
1 B	0.0	−4.1	13.2	−24.1
2 B	0.0	−4.5	15.4	−24.0
3 B	0.0	−2.6	14.8	−23.6
4 B	0.0	−3.2	16.0	−22.7
5 B	0.0	−2.9	14.8	−24.1
1 C	0.0	−1.1	19.7	−19.9
2 C	0.0	−2.9	21.9	−15.7
3 C	0.0	−3.0	24.4	−13.0
1 A$_F$	0.0	−3.2	17.0	−22.7
1 A$_{Cl}$	0.0	−3.8	16.2	−20.8
1 A$_{CN}$	0.0	−5.8	8.8	−21.1

ChemistryOpen

Full Papers
doi.org/10.1002/open.202000137

Chemistry Europe
European Chemical
Societies Publishing

position of the dienophile (Scheme 2) with bromine or methyl should have a detrimental effect on the activation energy and this seems to be independent of the nature of the substitution, although the strongest impact corresponds to methyl substituent (**TS3A**). Experimentally, the reaction of the 9-(1-methoxyethyl)-anthracene, an anthracene template similar to that used here, gives 89% yield in the cycloaddition with dienophile **1A** in benzene at 80 °C.[7] However, when the dienophile is changed to **2A** and **3A** the yield decreases to 82 and 84%, respectively, indicating a slightly less efficient reaction.[7] In the case of our calculations the activation energies seem to account for this loss of reactivity when the maleic anhydride is substituted by −Br and −CH$_3$. Nevertheless, we are aware that these substituents do not account for all electronic effects we must evaluate when different substituted olefins are used in DA reactions. So, in order to further understand the effect of substituents at R$_4$ in maleic anhydrides, we carried out additional calculations by varying R$_4$ with −F, −Cl and −CN, which will provide a more detailed role of the electron withdrawing (EWG) groups on the cycloaddition reactivity. The results are shown in Table 1 and the optimized structures of the RCs and TS structures corresponding to those maleic anhydrides can be found in Figure S8 of the Supporting Information. As observed, the inclusion of a highly EWG group like −CN group at R$_4$ of maleic anhydride leads to a lower activation energy compared to **1A**. On the other hand, dienophiles **1A$_F$** and **1A$_{Cl}$** lead to transition states with energies that are slightly higher than that of **1A** and very similar to **2A** (with R$_4$=−Br). Given these energy differences, we may conclude that halogen substitution has no effect on the reactivity of the dienophiles. The effect of fluorine in the reactivity of DA cycloadditions has been addressed for many types of dienes and dienophiles since the mid-50s.[53] Even when we might expect an acceleration of the reactions due to the electron withdrawing nature of fluorine, the opposite effect has been observed in the experiments, which has been supported by calculations.[54–56] This is in part due to the fact that the mesomeric effect (+M) in fluorine sometimes overpasses the electron withdrawing effect (−I) and, therefore, there is an increase in the electron density of the C=C bond compared to the unsubstituted olefin. For chlorine and bromine, the information available in the literature is scarce, but a combined experimental and computational report of DA cycloadditions between chiral α-halo-enones with cyclic and acyclic dienes suggested that halogen substitution lead to higher activation energies and, thus, to less efficient reactions.[57] The results obtained here are in agreement with these earlier contributions that show that halogen substituents should be detrimental to the reaction efficiency.

In the set of maleimides we evaluated both the effect of the R group at the N heteroatom and the substitution at R$_4$ position with −Br (Scheme 2). In this group, the activation energies for the unsubstituted maleimides (**TS1B**, **TS3B** and **TS5B**) varies in a range of computational accuracy ($\Delta\Delta G^{\neq}_{298}$ = 1.6 kcal mol^{-1}), which may suggests that the R substituent at the heteroatom has no effect on the activation energies, in agreement with the experimental results obtained by Adams and co-workers.[14] For −Br substituted maleimides the energy barriers increase slightly

by 2.2 and 1.2 kcal mol^{-1} for **TS2B** and **TS4B**, respectively, when compared to **TS1B**. Interestingly, when one compares dienophiles in the group of maleic anhydrides with those in the group maleimides having similar substitution patterns (**TS1A** with **TS1B**, **TS3B** and **TS5B** on one hand, and **TS2A** with **TS2B** and **TS4B** on the other hand), we observe very similar transition state energies, indicating that the activation energies are not only independent of the R group but also of the heteroatom at the five-member ring. These results are in agreement with experimental data from DA cycloadditions between 9-(1-methoxy-2,2,2-trifluoroethyl) anthracene and dienophiles **1A** and **1B**, which gave practically the same yield (75–76%) in benzene at 80 °C.[7]

For the last set of dienophiles, as in the previous cases, the lower energy barrier is associated with the non-substituted lactone (**TS1C**, $\Delta G^{\neq}_{298}$ = 19.7 kcal mol^{-1}), while for **TS2C** and **TS3C** the energies are 2.2 and 4.7 kcal mol^{-1} higher, respectively. Comparing the energy barriers calculated for **TS1A/TS1C**, **TS2A/TS2C** and **TS3A/TS3C** pairs we can observe the effect of changing a carbonyl (C=O) substituent at R$_5$ (Scheme 2) by an acetoxy group. In this case, the lactones group shows activation energies that are 4.8–5.5 kcal mol^{-1} higher in energy than those of the maleic anhydride group. This effect must be attributed to the higher steric perturbation at the transition states with the acetoxy groups because the carbon atom bearing this group in the dienophile is a sp^3 carbon.

Overall, the structures and energies of the minima and transition states along the reaction paths for DA cycloadditions are sensitive to the nature of the substituent of the incoming dienophile when approaching the anthracene template. In general, for maleic anhydrides halogen substitution at R$_4$ increases the activation energy compared to the unsubstituted dienophile, although within the set of halogens (−F, −Cl, −Br) there is no effect on the activation energies. Only the highly EWG cyanide group lowers the energy barrier with respect to the unsubstituted dienophile, as reported previously in many experimental and theoretical contributions.[38,58–62] For maleimides, we observe that the calculated activation energies are independent on both the N heteroatom at the five-member ring and the R group attached to it. Finally, for the lactones group, we observe the highest activation energies, with similar trends to those observed for the maleic anhydrides.

2.2. Frontier Molecular Orbitals and Charge-Transfer Analysis

Frontier molecular orbitals play an important role in DA reactions since they seem to control the cycloaddition process. The reactions between **ANT** and the eleven dienophiles studied here proceed through a DA cycloaddition of normal electron demand. Indeed, calculations of HOMO$_{diene}$-LUMO$_{dienophile}$ versus HOMO$_{dienophile}$-LUMO$_{diene}$ gaps indicate that the former is much lower than the second one (Table S4 of Supporting Information). When needed, for the inverse electron demand reaction the HOMO-1 of the dienophile was used since it has the proper symmetry to interact with the LUMO of **ANT**. Figure 3 shows a qualitative evolution of the FMO from separate reactants to the
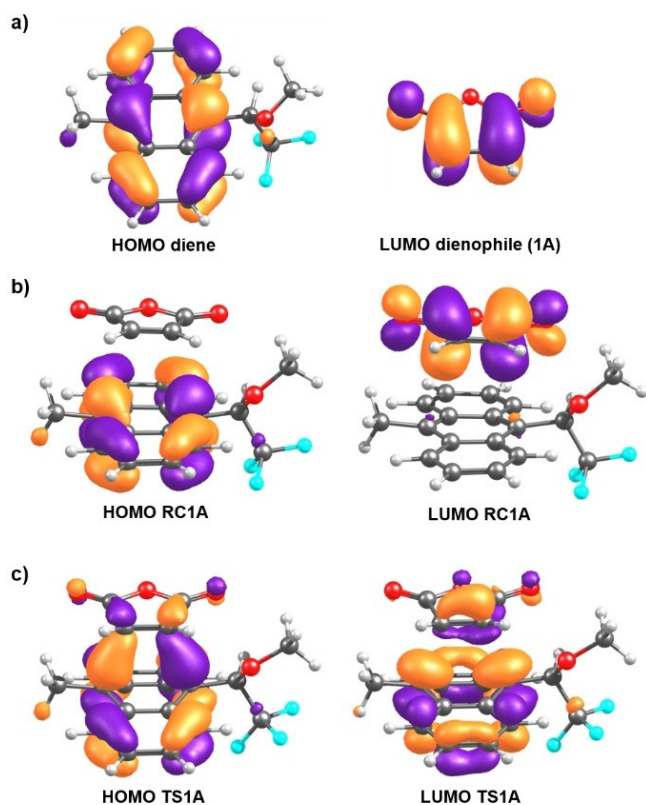
ChemistryOpen

Full Papers
doi.org/10.1002/open.202000137

Chemistry
Europe
European Chemical
Societies Publishing

Figure 3. Frontier molecular orbitals (FMO) of the stationary points for the reaction **ANT** and dienophile **1 A**; a) separate reactants; b) reactant complex; c) transition state structure. FMO were obtained at the M06-2X/TZVP//M06-2X/6-311 + + G(d,p) level of theory. Contour isovalue 0.04 au.

C_4–C_5 pairs, but antibonding between C_2–C_5 and C_3–C_4 (see Scheme 2 for atom numbering), leading to an overall antibonding character of the orbital.

Figure 3b shows the FMO of **RC1A**. As observed, in this complex the HOMO and LUMO are mainly localized on the individual moieties as in the separate reactants, indicating that no CT is taking place on these molecular complexes. In the case of the lactones group, the HOMO and LUMO are located on the anthracene ring while LUMO + 1 is localized on the dienophile moiety (see Figure S12 of the Supporting Information). The electronic features of the RCs and its relationship with the individual reactants and the transition states are better understood if one looks to what happens when the HOMO-LUMO gap at the RCs (HOMO-LUMO + 1 for the lactones) is plotted against the normal electron demand considering the FMO of separate reactants (Table S4 of the Supporting Information) and the CT at the corresponding TS structures. These outcomes are shown in Figure S16 of Supporting Information. Nearly perfect relationships are found for both correlations ($R^2 > 0.94$), indicating that the electronic features of the separate reactants are preserved in the molecular complexes (Figure S16a) and that the gap between FMO at the RCs is directly related to the CT at the TS structures (Figure S16b).

Figure 4 shows a nearly perfect linear relationship between the amount of CT and the HOMO-LUMO gap at the corresponding TS for the maleic anhydrides and maleimides group ($R^2 = 0.99$), while for the acetoxy lactones group there is no correlation (Figure 4a). The perfect linear relationship in the maleic anhydrides is even kept when considering substituted dienophiles $1A_F$, $1A_{Cl}$, and $1A_{CN}$ (Figure 4b). The expected trend that dictates that the smaller the HOMO-LUMO gap at the TS, the higher the extent of CT, is only fulfilled by the maleic anhydride and maleimide groups.

On the other hand, Figure 5 shows the relationships of the amount of CT and the HOMO-LUMO gap at the TS structures with the activation energies ($\Delta E^{\ddagger}$) for the three groups of dienophiles. According to the literature, an acceleration of the reaction must be expected with the increase of CT at the TS.[50]
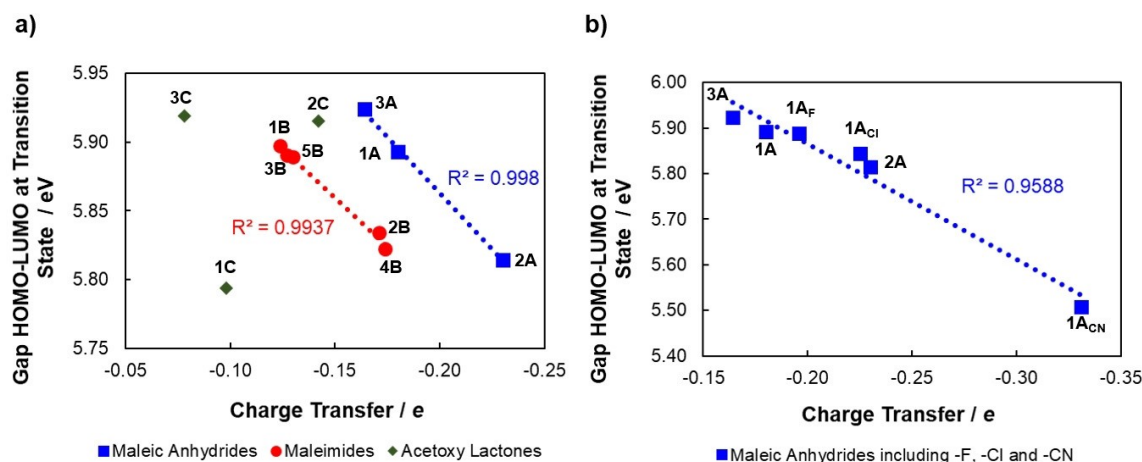
transition state structure for dienophile **1 A** as an example. All other dienophiles present similar behavior and their FMO may be seen in Figures S9–S15 of the Supporting Information. The main orbital interaction between reactants involves the HOMO of **ANT** and the LUMO of the dienophile (Figure 3a). The latter orbital is mainly localized on the carbon atoms of the five-member ring, with bonding interaction between C_2–C_3 and

Figure 4. Plot of the CT versus a) the HOMO-LUMO gap at the TS structures for three groups of dienophiles considered here; b) the HOMO-LUMO gap at the TS structures of maleic anhydrides $1A_F$, $1A_{Cl}$, and $1A_{CN}$. Calculations were performed at the M06-2X/TZVP//M06-2X/6-311 + + G(d,p) level of theory.
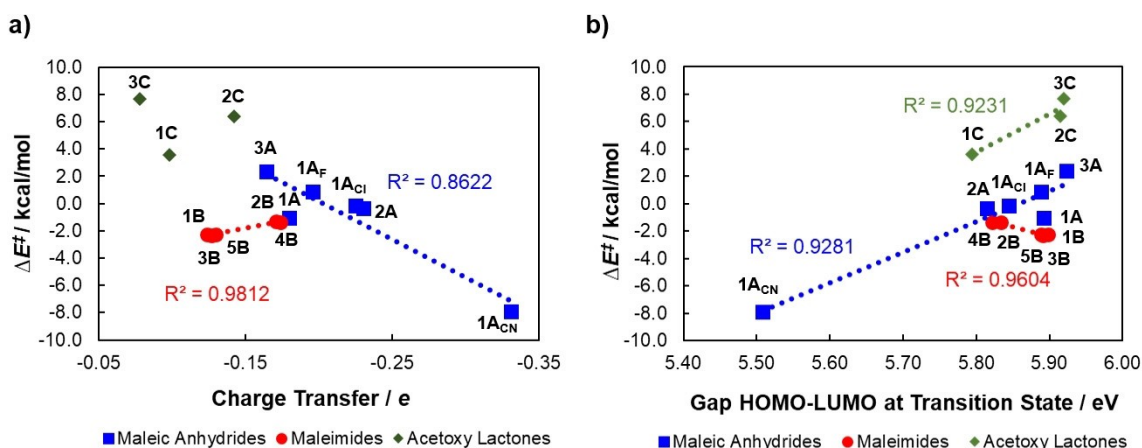
ChemistryOpen

Full Papers
doi.org/10.1002/open.202000137

Chemistry Europe
European Chemical
Societies Publishing

Figure 5. Plot of the a) CT and b) HOMO-LUMO gap at TS versus the activation energy ($\Delta E^{\pm}$) for all dienophiles considered here. Calculations were performed at the M06-2X/TZVP//M06-2X/6-311 $+ +$ G(d,p) level of theory.

For maleic anhydrides and maleimides very good to perfect linear correlations are found (Figure 5a, $R^2 = 0.86$ and 0.98, respectively), although the slopes of the curves for the two groups have different signs. The expected trend is only fulfilled by the maleic anhydrides group, suggesting that the activation energy may be controlled by the amount of charge transferred from the diene to the dienophile during the cycloaddition. This effect has already been observed in polar DA reactions between cyclopentadiene and a variety of substituted ethylene dienophiles.[50] For the maleimides, the slope of the curve indicates that increasing the CT at the TS also increase the activation energy. In the case of the acetoxy lactones group no correlation was found, indicating the CT does not have any influence on the activation energies. However, when plotting the HOMO-LUMO gap at the TS against the activation energies (Figure 5b), nearly perfect linear relationships are found for all three groups ($R^2 > 0.92$). For maleic anhydrides and the acetoxy lactones groups the slope of the curve indicates that low activation energies are associated with small gaps between the FMO at the TS structures, but the opposite trend is observed for the maleimides group.

In order to try to understand why the acetoxy lactones group does not show any correlation between charge transfer and activation energies, we also compute the orbital overlap (S) at each one of the TS structures. The results in Table 2 clearly indicate that orbital overlap is not a key factor in determining the activation energies and CT, since it is nearly constant along the three group of dienophiles. In view of these results, there should be another factor that determines the activity of the lactones group.

2.3. DA Cycloadditions from the ASM Perspective

The ASM was applied to the present DA cycloadditions between **ANT** and all dienophiles, considering the RC and TS from separate reactants. The results of the ASM calculations for the generation of the RCs are shown in Table S5 of the Supporting

Table 2. HOMO-LUMO gaps at the transition states and orbital overlap for all reactions considered here calculated at the M06-2X/TZVP//M06-2X/6-311 $+ +$ G(d,p) level of theory.

Dienophile	HOMO-LUMO Gap at TS (eV)	HOMO-LUMO Gap at separate reactants (eV)	Orbital Overlap (S, au)
1 A	5.89	4.35	0.16
2 A	5.81	4.16	0.16
3 A	5.92	4.64	0.16
1 A$_F$	5.89	4.27	0.16
1 A$_{Cl}$	5.84	4.16	0.16
1 A$_{CN}$	5.51	3.38	0.16
1 B	5.90	4.87	0.15
2 B	5.83	4.66	0.16
3 B	5.89	4.86	0.15
4 B	5.82	4.65	0.16
5 B	5.89	4.87	0.15
1 C	5.79	5.57	0.17
2 C	5.91	5.33	0.17
3 C	5.92	5.85	0.18

Information. As can be observed, the strain energies developed on going from isolated reactants to the RCs range from 0.2 to 1 kcal mol^{-1}, indicating that there is no significant distortion of the fragments (diene and dienophile) in the RCs. Conversely, the interaction energies range from -20.4 to -14.8 kcal mol^{-1}, meaning that most of the reaction energies for the formation of the RCs come from the interaction between fragments. Regarding the TS structures, the discussion will be carried out separately for the three groups of dienophiles. In the group of the maleic anhydrides neither the interaction energy nor the strain energy play a significant role on determining the activation energies (see Figure S17 of the Supporting Information). The interaction energies show a very modest correlation ($R^2 = 0.6$) with the activation energies, whereas for the strain energies the data are more scattered, leading to an even worst correlation. In view of this data, we may conclude that the DA cycloaddition of maleic anhydrides with **ANT** must be controlled by the extent of CT and the HOMO-LUMO gap at the TS, as revealed in Figures 4 and 5.

ChemistryOpen

Full Papers
doi.org/10.1002/open.202000137

Chemistry
Europe
European Chemical
Societies Publishing

In the case of maleimides, the ASM calculations reveal that both the strain (Figure 6a) and interaction energies (Figure 6d) play a role in determining the activation energies. The total strain energies (Figure 6a, $R^2 = 0.994$) range from 24.7 to 30.8 kcal mol^{-1}. The TS structures for unsubstituted maleimides (**TS1B**, **TS3B** and **TS5B**) shows strain energies of 24.7–25.2 kcal mol^{-1} while those of substituted maleimides (**TS2B** and **TS4B**) presents strain energies of 30.7 and 30.1 kcal mol^{-1}, respectively, indicating that the R group at the N heteroatom has no influence on the distortion energies. On the contrary, it is the −Br substituent at R4 (Scheme 2) that introduce the difference in the strain energies. In general, the total strain

energies for the TS structures of substituted maleimides is 5.5 kcal mol^{-1} higher than those of unsubstituted ones. When looking at the origin of these differences for the strain energies we must anticipate that lower strain energies may be associated with early TS structures on the cycloaddition PES.[63] However, in this case is difficult to classify the TS structures for maleimides **1B-5B** as early or late since the substituted TS structures are asynchronous (see Figure 3), leading to two different C⋯C distances ($d1 = 2.17$–2.18 Å and $d2 = 2.35$–2.36 Å), which average value is actually the same as that for the synchronous TS structures (2.25–2.26 Å). The true origin of the calculated strain energies is evident when we look at the individual components
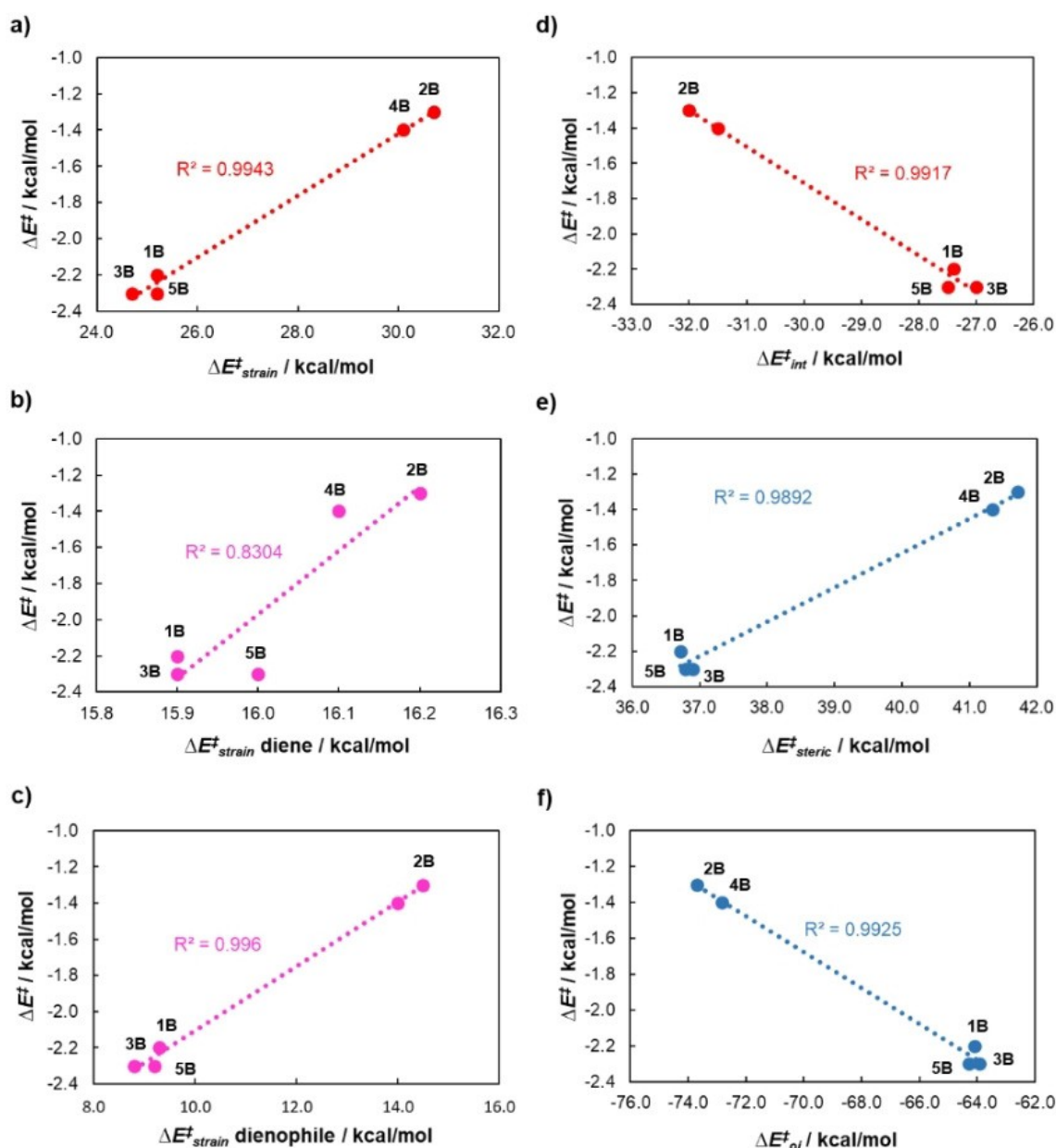

Figure 6. Plots of the a) total strain energies ($\Delta E^{\ddagger}_{strain}$) and their components b) the strain energies of the diene and c) the strain energies of the dienophile versus the activation energy ($\Delta E^{\ddagger}$); plots of the d) interaction energies ($\Delta E^{\ddagger}_{int}$) and their components e) the steric repulsion energy and f) the orbital interaction energies versus the activation energy ($\Delta E^{\ddagger}$) for the group of maleimides. Calculations were performed at the M06-2X/TZVP//M06-2X/6-311++G (d,p) level of theory.

ChemistryOpen

Full Papers
doi.org/10.1002/open.202000137

Chemistry Europe
European Chemical
Societies Publishing

of the total strain energies (Figure 6b and **6c**). The ASM calculations shows that the strain energies for the diene fragment are neatly constant (between 15.9 and 16.2 kcal mol^{-1}), suggesting that the distortion at the diene does not play a role on the activation energies. On the other hand, the distortion at the dienophile fragment is the one which controls the activation energies (Figure 6c, $R^2 = 0.996$). For the unsubstituted maleimides, the strain energies of the dienophile fragment at the TS structures range from 8.8 to 9.3 kcal mol^{-1}, while for the −Br substituted maleimides the dienophile strain energies are 14.0 and 14.5 kcal mol^{-1} (**TS4B** and **TS2B**, respectively). This means an increase of about 5 kcal mol^{-1} in the dienophile strain energy only by changing a hydrogen by bromine. This is because it is more difficult to distort the heavy Br atom from the isolated reactants to the geometry of the transition state. Indeed, the N–C–C–R4 dihedral angle for isolated dienophiles **1B**–**5B** are zero or close to zero, indicating perfectly planar structures. However, when approaching to the anthracene template, orbital interactions take place by pushing away the atoms attached to the C═C double bond of the dienophile. For the unsubstituted maleimides, the N–C–C–R4 dihedral angles of the dienophile fragment of the TS structures reach a value of 22—23°, while the N–C–C–R4 dihedral angles of the substituted maleimides are about 30°, thus indicating that substituted maleimides are more distorted that the unsubstituted ones in the transition states.

Figure 6d show that low activation energies are associated with less stabilizing interaction energies at the TS ($R^2 = 0.992$). The most stabilizing interaction energies are associated to the substituted maleimides (**TS2B** and **TS4B**), with values of about 32 kcal mol^{-1}, while interaction energies for unsubstituted maleimides show a nearly constant value of *ca.* 27 kcal mol^{-1}. The difference in interaction energies between substituted and unsubstituted maleimide TS structures (~4.5 kcal mol^{-1}) is similar to the difference in distortion energy, thus suggesting that the lowering in interaction energies for the substituted maleimides almost offset the increasing in strain energies. When the interaction energy is partitioned into its components, we observe a careful balance of the steric repulsion (Figure 6e) and orbital interaction terms (Figure 6f). Figure 6e indicates that unsubstituted maleimides show the lowest steric repulsion energies ($R^2 = 0.989$), which agrees with the distortion energies of the dienophile fragments (Figure 6c). Conversely, Figure 6f implies that low activation energies must be related to the less stabilizing orbital energies ($R^2 = 0.992$). These results agree with those obtained from the analysis of charge transfer and HOMO-LUMO gap (Figure 5), where low activation energies were associated with less extent of charge transfer and higher orbital energy gaps between FMO.

Finally, the strain and interaction energies for the acetoxy lactones group are depicted in Figure 7. The correlation between the activation energies and the interaction energies at the TS structures are rather modest ($R^2 = 0.557$), suggesting that interaction energies do not play a significant role on the activation energies of the DA cycloadditions. Nevertheless, when looking at the correlation between the strain energies and activation energies a much better correlation ($R^2 = 0.848$) is observed. The total strain energy for **TS1C**, **TS2C** and **TS3C** are 27.4, 35.1 and 34.6 kcal mol^{-1}, respectively. The lower strain energy for **TS3C** compared to **TS2C** is due the lower strain energy of the dienophile fragment in **TS3C**. Indeed, the strain energies for the dienophile fragments are 10.6, 17.5 and 16.1 kcal mol^{-1}, respectively for **1C**, **2C** and **3C**, leading to a relatively modest relationship ($R^2 = 0.74$). Nevertheless, the activation energies seem to be controlled by the distortion of the diene fragment ($R^2 = 0.954$). The strain energies of the diene fragment for **TS1C**, **TS2C** and **TS3C** are 16.8, 17.6 and 18.5 kcal mol^{-1}, respectively. The diene strain energies increase monotonically from **1C** to **2C** and to **3C** with very modest energy differences (less than 1 kcal mol^{-1}), so the origin of these differences must be due to subtle changes in the geometry of the diene at the TS structures. A possible explanation is that the average C···C distances in the less distorted **TS1C** are larger than the average C···C distances in **TS2C** and **TS3C**, suggesting that the former may be an early TS structures (less distorted) while the later seems to be associated with late TS structures (more distorted).

Overall, the results obtained from the ASM calculations shed light into some key features not explored before for the DA reactions studied here. On one hand, the activation energies of DA cycloadditions with maleic anhydrides are not controlled neither by strain nor activation energies, but rather by an interplay of CT and HOMO-LUMO gap orbital energies. In the case of maleimides, the activation energies are under dual control by the strain and the interaction energies, which in turn reproduce the results coming from the CT and the HOMO-LUMO gap orbital energy analysis. In the case of the acetoxy lactones group, the activation energies seem to be controlled by the distortion energy needed to deform the isolated reactants to the geometry of TS, and in this case the distortion of the anthracene fragment at the TS appears to play a more critical role on the activation energies.

2.4. Effect of Catalysts on the DA Cycloadditions

It is well known that Diels Alder cycloadditions are affected by the presence of catalysts.[64] For the type of reactions studied here involving chiral anthracenes, Snyder demonstrated that Lewis acid catalyzed cycloadditions proceed at lower temperature (compared to the uncatalyzed reaction) and led to higher diastereoselectivity.[7] The Brønsted acid catalysis has been computationally tackled before for the DA cycloaddition between maleic anhydride and 2,5-dimethylfurane[65] using H$^+$ as a model catalyst. Here, we adopted a similar approach in order to assess the effect of a catalyst in the present reactions. Accordingly, we carried out gas phase calculations of DA cycloadditions between **ANT** and maleic anhydrides **1A**, **2A** and **3A** in presence of a proton (H$^+$) as a model of a Brønsted acid. First, we evaluated the most favorable protonation sites of both **ANT** and the dienophiles considered (see Figure S18 of the Supporting Information). This is because both the dienophiles and/or the diene may potentially bind H$^+$ on different positions. In the case of **ANT** (Figure S18a), three different
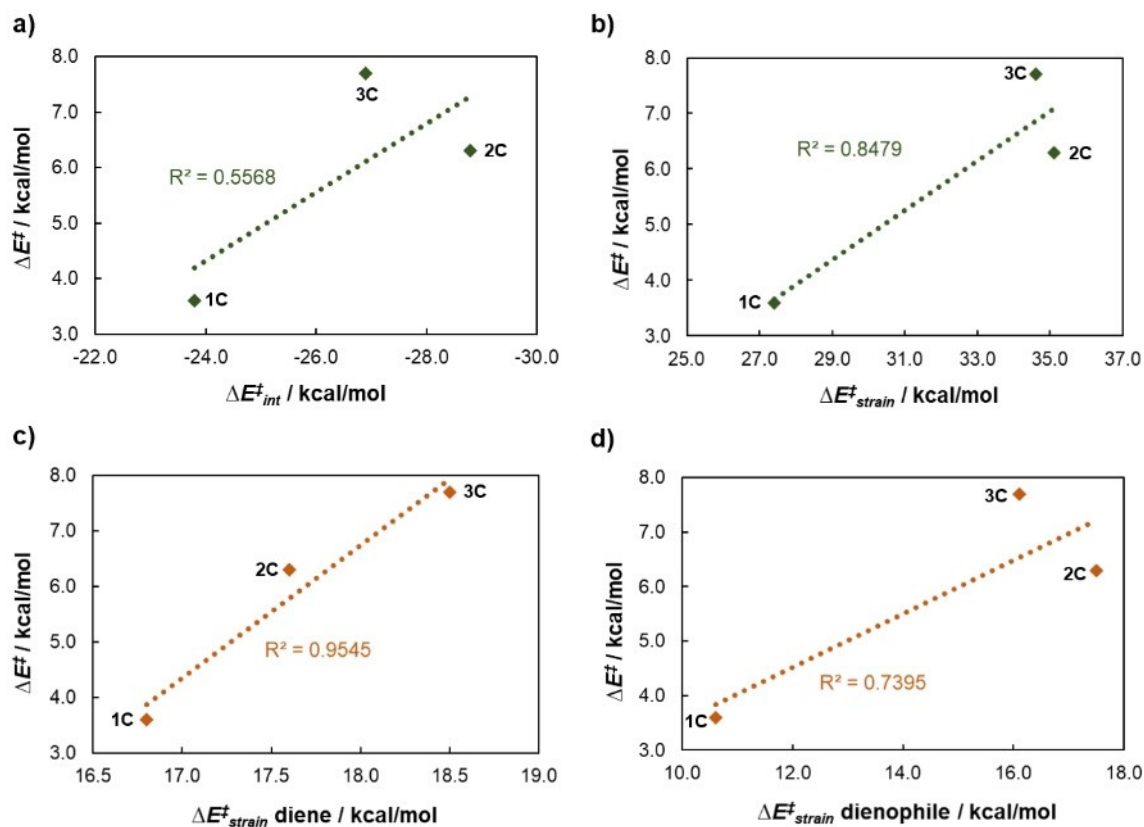
ChemistryOpen

Full Papers
doi.org/10.1002/open.202000137

Chemistry Europe
European Chemical
Societies Publishing

Figure 7. Plots of the a) interaction energies ($\Delta E^{\ddagger}_{int}$) and b) strain energies ($\Delta E^{\ddagger}_{strain}$) versus the activation energy ($\Delta E^{\ddagger}$) for the group of acetoxy lactones. The individual components of the strain energies are also shown for c) diene and d) dienophile. Calculations were performed at the M06-2X/TZVP//M06-2X/6-311 + +G(d,p) level of theory.

protonation sites were considered for the formation of the corresponding carbocation: C1, C2 and C4 (shown by a red circle in Figure S18a and the corresponding cation with a plus, +). Among all explored sites, the most favorable one is C1 although C4 shows a very similar relative energy. On the other hand, protonation at C2 leads to a higher-energy carbocation. We even considered protonation of the diene on the metoxy and trifluoromethyl groups, but this leads to much high-energy carbocations (not shown in Figure S18). In the case of the dienes, we explored protonation of the carbonyl oxygens and the oxygen belonging to the five-member ring of the maleic anhydride system (Figure S18b). The latter option led an opening of the ring structure, thus suggesting that this protonation does not give any DA product, in agreement with the results from Doren et al.[65] Protonation of maleic anhydride **1A** on the carbonyl oxygen lead to two possible isomers depending on the orientation of the H$^+$ cation. The configuration with H$^+$ pointing towards the O heteroatom is the lowest energy structure, probably because the presence of a H-bond interaction between them (the H$^+\cdots$O distance is 2.36 Å). In view of these preliminary results, we decided to select the structures **ANT-H$^+$-1** and **1A-H$^+$-1** (and analogue structures for **2A** and **3A**) as the starting reactants to model the catalyzed DA process. In a second step, we evaluated two options for the possible Brønsted acid catalyzed reactions. The option **1** corresponds to

the reaction **ANT**+n**A-H$^+$-1** and the option **2** corresponds to **ANT-H$^+$-1**+n**A** (in all cases $n = 1$, **2** and **3**). The FMO gaps for two above-mentioned options are shown in Table 3, where normal an inverse electron demand are considered, and the individual molecular orbitals of **ANT-H$^+$-1** and n**A-H$^+$-1** are shown in Figure S19 of the Supporting Information. As observed, while option **1** follows a normal demand (HOMO$_{diene}$-LUMO$_{dienophile}$) option **2** is characterized by an inverse demand (HOMO$_{dienophile}$-LUMO$_{diene}$).

Figure 8 shows the Gibbs energy profiles for the two options of the acid catalyzed cycloaddition between **ANT** and **1A** as example, and the comparison with the uncatalyzed reaction. As noted in Figure 8a, option **2** is associated with very high activation energies compared to the option **1**. The latter shows the lowest in energy profile, meaning that the proton prefers to interact exclusively with maleic anhydride. The presence of the proton on the carbonyl oxygen of **1A** induces a

Table 3. Frontier Molecular Orbital (HOMO-LUMO) gaps for the Brønsted acid catalyzed reactions considered here, calculated at the M06-2X/TZVP//M06-2X/6-311 + +G(d,p) level of theory.

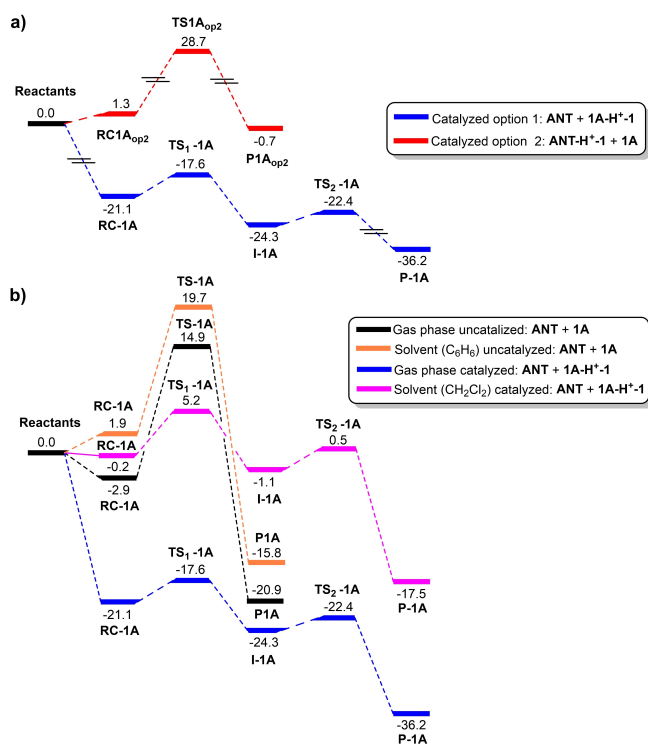|	Option 1	Option 2
Normal demand (eV)	−1.54	8.77
Inverse demand (eV)	15.03	6.66

Figure 8. Gibbs energy profiles at 298 K (in kcal mol^{-1}) of the DA cycloaddition between **ANT** and maleic anhydride **1 A**, considering a) the two gas phase catalyzed pathways where the Brønsted acid (H$^+$) is placed on **1 A** (option 1, blue profile) and on **ANT** (option 2, red profile), and b) the comparison between uncatalyzed and catalyzed reactions in gas phase and solvent. In all cases, the origin of energies are the separate reactants. All calculations were performed at the M06-2X/6-311++G(d,p) level of theory.

shift of the reaction mechanism from concerted to stepwise, showing two TS structures, both of them being below separate reactants. These results suggest that when considering gas phase energies the Brønsted acid catalyzed cycloadditions studied here proceed without energy barriers, in agreement with the results of Doren *et al.*[65] However, we must anticipate that the solvent may have a critical role on the relative energies for the most favorable catalyzed mechanism.

Therefore, we carried out single-point energy calculations in solvent (benzene and dichloromethane) based on the M06-2X/6-311++G(d,p) geometries. Comparison between the energetics in gas phase and in solvent for the uncatalyzed and catalyzed reactions (Figure 8b) shows the impact of considering the solvent in the studied pathways. In this case, the catalyzed reaction in dichloromethane shows an activation energy of 5.2 kcal mol^{-1} for the first TS structure, whereas the second TS has a lower energy. In contrast, the uncatalyzed reaction shows an activation energy of about 20 kcal mol^{-1} in benzene. Calculations for the catalyzed DA cycloadditions between **ANT** and dienophiles **2 A** and **3 A** in gas phase and solvent shows similar trends (Figure S20 of the Supporting Information). These results indicate that the catalyst is a critical parameter that affects the reactivity of DA cycloadditions involving chiral anthracenes.

We also computed the FMO of the two TS structures of the most favorable catalyzed pathway for the three considered dienophiles, (see Figure S21 of the Supporting Information). The shape of the molecular orbitals involved in the CT process in the first transition state are similar to the uncatalyzed case (Figure 3c), showing a bonding component between the two pairs of carbon atoms of the two moieties (C9$_{diene}$—C4$_{dienophile}$ and C10$_{diene}$—C3$_{dienophile}$, see Scheme 2 for atom numbering). Interestingly, the second TS structures show only a reduced bonding interaction (between C9 of the diene and C4 of dienophile). This situation is consistent with the computed CT at the TS structures, calculated as the summation of the NPA charges at the dienophile fragment, which shows that the larger amount of electrons are transferred in the first TS structure. This CT at the first TS structures also shows an excellent correlation ($R^2 = 1$) when plotting against the HOMO-LUMO gap at the corresponding TS, as shown in Figure S22 of the Supporting Information. Remarkably, the relationship between CT and HOMO-LUMO gaps for the set of maleic anhydrides is the same as that found for the uncatalyzed reaction, including the relative ordering of the dienophiles (Figure 3a). These results suggest that in the catalyzed reaction the electronic properties at the TS structures are kept compared to the uncatalyzed one, even though there is an increase of CT and a lowering of the HOMO-LUMO gap.

3. Conclusions

In this contribution, we carried out extensive DFT calculations in order to study the Diels Alder cycloadditions between a chiral template 10-methyl-9-(1-methoxy-2,2,2-trifluoroethyl) anthracene and a series of dienophiles based on maleic anhydrides, maleimides and acetoxy lactones. The reaction mechanism and the energetics of the reactions were studied at the M06-2X/6-311++G(d,p) level of theory. All reactions were found to proceed via concerted transition states with varying degrees of synchronicity depending upon the substitution pattern and not on the nature of the substituent itself. We found that all reactions are characterized by the presence of molecular complex prior to the transition state structure. The energetics of the cycloadditions are extremely sensitive to substitution of the dienophile. Substitution of maleic anhydrides at R$_4$ with halogen atoms (—F, —Cl, —Br) or methyl leads to higher activation energies when compared to the unsubstituted one, which is supported by the experiments available to date. Only substitution with the highly electron withdrawing —CN group lead to lower energy barriers. We also observed that for maleimides the calculated energy barriers are not only independent on the heteroatom on the five-member ring skeleton of the dienophile but also on the length of the alkyl substituent attached to it.

The analysis of frontier molecular orbitals (M06-2X/TZVP//M06-2X/6-311++G(d,p)) indicates that the Diels Alder cycloadditions studied here proceed under normal electron demand dominated by the interaction between the HOMO of the anthracene template and the LUMO of the dienophiles. We

found a very good linear relationship between the amount of charge transfer and the activation energy for the maleic anhydrides group, in such a way the larger the extent of charge transfer at the transition state, the lower the activation energy. For maleimides there is a nearly excellent relationship between charge transfer and the activation energies, but the slope of the curve is opposite to that of the maleic anhydrides, indicating that increasing the charge transfer at the transition state is accompanied by higher activation energies. For the acetoxy lactones no correlation was found, and the analysis of orbital overlap indicates that this parameter is not crucial in determining the reactivity of this group. The application of the Activation Strain Model to the reactions considered here shed light on some unexplored features of the cycloadditions. On one hand, the formation of the reactant complex is controlled by the interaction energy between fragments (diene and dienophile) with practically negligible influence of the distortion energies. On the other hand, when looking at the activation energies, we found that the reactivity in the maleic anhydrides group is not controlled neither by interaction nor distortion energies. Instead, for this group the reactivity seems to be controlled by charge transfer effects at the transition states. For maleimides, there is a dual control of the interaction and distortion energies on the activation energies. The energy decomposition analysis indicate that the interaction energies are composed by a balance between the orbital interaction energy and steric energy with opposite trends. For the acetoxy lactones, the reactivity is controlled by distortion energy of the molecular fragments, and the analysis of the contributions indicates that distortion of the diene fragment plays a more significant role on determining the activation energies.

Finally, we explored the effect of a Brønsted acid catalyst (modeled as a H^+) in the reaction mechanism and energetics of the reactions for the maleic anhydrides group. Calculations indicate that the proton prefers to interact with the dienophile. In this case, the reaction mechanism shifts from concerted to stepwise, with two transition state structures, although the first one is the most important in terms of energies and charge transfer effects. The calculated gas phase energies indicate that the cycloaddition proceed with no energy barrier, but inclusion of solvent rise the energy of all stationary points, thus leading to Gibbs energy barriers between 2 and 9 kcal mol^{-1}. Comparison with the energetics of the uncatalyzed reactions shows the benefits of a catalyst on the Diels Alder cycloadditions studied here.

Acknowledgments

Conflict of Interest

The authors declare no conflict of interest.

[1] F. Fringuelli, A. Taticchi, *The Diels-Alder Reaction: Selected Practical Methods*; Wiley, J. & S., Ed.; John Wiley & Sons.: Baffins Lane, Chichester, **2002**.
[2] K. N. Houk, J. Gonzalez, Y. Li, *Acc. Chem. Res.* **1995**, *28* (2), 81–90.
[3] T. J. Brocksom, J. Nakamura, M. L. Ferreira, U. Brocksom, *J. Braz, Chem. Soc.* **2001**, *12*, 597–622.
[4] D. H. Ess, G. O. Jones, K. N. Houk, *Adv. Synth. Catal.* **2006**, *348*, 2337–2361.
[5] J. A. Funel, S. Abele, *Angew. Chem. Int. Ed.* **2013**, *52*, 3822–3863; *Angew. Chem.* **2013**, *125*, 3912–3955.
[6] M. S. Corbett, X. Liu, A. Sanyal, J. K. Snyder, *Tetrahedron Lett.* **2003**, *44*, 931–935.
[7] A. Sanyal, J. K. Snyder, *Org. Lett.* **2000**, *2*, 2527–2530.
[8] E. T. Akin, M. Erdogan, A. Dastan, N. Saracoglu, *Tetrahedron* **2017**, *73*, 5537–5546.
[9] M. G. Teixeira, E. S. Alvarenga, *Magn. Reson. Chem.* **2016**, *54*, 623–631.
[10] M. J. S. Dewar, *J. Am. Chem. Soc.* **1984**, *106*, 209–219.
[11] M. Linder, T. Brinck, *J. Org. Chem.* **2012**, *77*, 6563–6573.
[12] B. Alcaide, P. Almendros, C. Aragoncillo, *Chem. Rev.* **2007**, *107*, 4437–4492.
[13] K. L. Burgess, N. J. Lajkiewicz, A. Sanyal, W. Yan, J. K. Snyder, *Org. Lett.* **2005**, *7*, 31–34.
[14] H. Adams, T. M. Elsunaki, I. Ojea-Jiménez, S. Jones, A. J. H. M. Meijer, *J. Org. Chem.* **2010**, *75*, 6252–6262.
[15] R. A. Bawa, F. M. Gautier, H. Adams, A. J. H. M. Meijer, S. Jones, *Org. Biomol. Chem.* **2015**, *13*, 10569–10577.
[16] L. J. Andrews, R. M. Keefer, *J. Am. Chem. Soc.* **1955**, *77*, 6284–6289.
[17] J. C. C. Atherton, S. Jones, *Tetrahedron* **2003**, *46*, 9039–9057.
[18] H. Adams, S. Jones, A. J. H. M. Meijer, Z. Najah, I. Ojea-Jiménez, A. T. Reeder, *Tetrahedron: Asymmetry* **2011**, *22*, 1620–1625.
[19] A. Sanyal, Q. Yuan, J. K. Snyder, *Tetrahedron Lett.* **2005**, *46*, 2475–2478.
[20] N. Çelebi-Ölçüm, A. Sanyal, V. Aviyente, *J. Org. Chem.* **2009**, *74*, 2328–2336.
[21] S. Agopcan, N. Elebi-Ölüm, M. N. Üiik, A. Sanyal, V. Aviyente, *Org. Biomol. Chem.* **2011**, *9*, 8079–8088.
[22] I. Fernández, F. M. Bickelhaupt, *Chem. - An Asian J.* **2016**, *11*, 3297–3304.
[23] F. M. Bickelhaupt, K. N. Houk, *Angew. Chem. Int. Ed.* **2017**, *56*, 10070–10086; *Angew. Chem.* **2017**, *129*, 10204–10221.
[24] M. J. Frisch, G. W. Trucks, H. B. Schlegel, G. E. Scuseria, M. A. Robb, J. R. Cheeseman, G. Scalmani, V. Barone, B. Mennucci, G. A. Petersson, H. Nakatsuji, M. Caricato, X. Li, H. P. Hratchian, A. F. Izmaylov, J. Bloino, G. Zheng, J. L. Sonnenberg, M. Hada, M. Ehara, K. Toyota, R. Fukuda, J. Hasegawa, M. Ishida, T. Nakajima, Y. Honda, O. Kitao, H. Nakai, T. Vreven, J. A. Montgomery Jr, J. E. Peralta, F. Ogliaro, M. Bearpark, J. J. Heyd, E. Brothers, K. N. Kudin, V. N. Staroverov, R. Kobayashi, J. Normand, K. Raghavachari, A. Rendell, J. C. Burant, S. S. Iyengar, J. Tomasi, M. Cossi, N. Rega, J. M. Millam, M. Klene, J. E. Knox, J. B. Cross, V. Bakken, C. Adamo, J. Jaramillo, R. Gomperts, R. E. Stratmann, O. Yazyev, A. J. Austin, R. Cammi, C. Pomelli, J. W. Ochterski, R. L. Martin, K. Morokuma, V. G. Zakrzewski, G. A. Voth, P. Salvador, J. J. Dannenberg, S. Dapprich, A. D. Daniels, O. Farkas, J. B. Foresman, J. V. Ortiz, J. Cioslowski, D. J. Fox, Gaussian 09, Rev. D.01. *Gaussian 09, Rev. D.01;Gaussian Inc.: Wallingford, CT.* Gaussian Inc. Wallingford CT: Wallingford CT **2013**.
[25] Y. Zhao, D. G. Truhlar, *Theor. Chem. Acc.* **2008**, *120*, 215–241.
[26] R. B. J. S. Krishnan, J. S. Binkley, R. Seeger, J. A. Pople, *J. Chem. Phys.* **1980**, *72*, 650–654.
[27] D. Yepes, J. Valenzuela, J. I. Martínez-Araya, P. Pérez, P. Jaque, *Phys. Chem. Chem. Phys.* **2019**, *21*, 7412–7428.

[28] S. N. Pieniazek, F. R. Clemente, K. N. Houk, *Angew. Chem. Int. Ed.* **2008**, *47*, 7746–7749; *Angew. Chem.* **2008**, *120*, 7860–7863.

[29] F. Jensen, *Introduction to Computational Chemistry*, 2a edition., Wiley, J. & S., Ed., The Atrium, Southern Gate, Chichester, **2007**.

[30] A. Schäfer, H. Horn, R. Ahlrichs, *J. Chem. Phys.* **1992**, *97*, 2571–2577.

[31] A. E. Reed, F. Weinhold, *J. Chem. Phys.* **1983**, *78*, 4066–4073.

[32] A. E. Reed, R. B. Weinstock, F. Weinhold, *J. Chem. Phys.* **1985**, *83*, 735–746.

[33] T. Lu, F. Chen, *J. Comput. Chem.* **2012**, *33*, 580–592.

[34] K. Morokuma, *J. Chem. Phys.* **1971**, *55*, 1236–1244.

[35] T. Ziegler, A. Rauk, *Theor. Chim. Acta* **1977**, *46*, 1–10.

[36] F. M. Bickelhaupt, E. J. Baerends, *Reviews in Computational Chemistry*; Lipkowitz, K. B., Boyd, D. B., Eds.; Weinheim, **2000**; Vol. 15.

[37] K. E. Wise, R. A. Wheeler, *J. Phys. Chem. A* **1999**, *103*, 8279–8287.

[38] G. O. Jones, V. A. Guner, K. N. Houk, *J. Phys. Chem. A* **2006**, *110*, 1216–1224.

[39] M. S. Liao, Y. Lu, S. Scheiner, *J. Comput. Chem.* **2003**, *24*, 623–631.

[40] M. H. Howard, V. Alexander, W. J. Marshall, D. C. Roe, Y. J. Zheng, *Synthesis (Stuttg).* **2003**, *68*, 120–129.

[41] J. E. Frey, A. M. Andrews, S. D. Combs, S. P. Edens, J. J. Puckett, R. E. Seagle, L. A. Torreano, *J. Org. Chem.* **1992**, *57*, 6460–6466.

[42] V. D. Kiselev, J. G. Miller, *J. Am. Chem. Soc.* **1975**, *97*, 4036–4039.

[43] R. Sustmann, M. Dern, R. Kasten, W. Sicking, *Chem. Ber.* **1987**, *120*, 1315–1322.

[44] R. Sustmann, H.-G. Korth, U. Nüchter, J. Siangouri-Feulner, W. Sicking, *Chem. Ber.* **1991**, *124*, 2811–2817.

[45] D. Suárez, J. A. Sordo, *Chem. Commun.* **1998**, 385–386.

[46] G. Berionni, P. A. Bertelle, J. Marrot, R. Goumont, *J. Am. Chem. Soc.* **2009**, *131*, 18224–18225.

[47] K. L. Handoo, Y. Lu, V. D. Parker, *J. Am. Chem. Soc.* **2003**, *125*, 9381–9387.

[48] Z. Yoshida, T. Kobayashi, *Tetrahedron* **1970**, *26*, 267–271.

[49] J. E. Frey, A. M. Andrews, D. G. Ankoviac, D. N. Beaman, L. E. Du Pont, T. E. Elsner, S. R. Lang, M. A. Oosterbaan Zwart, L. A. Torreano, R. E. Seagle, *J. Org. Chem.* **1990**, *55*, 606–624.

[50] L. R. Domingo, J. A. Sáez, *Org. Biomol. Chem.* **2009**, *7*, 3576–3583.

[51] B. J. Levandowski, K. N. Houk, *J. Org. Chem.* **2015**, *80*, 3530–3537.

[52] M. G. Evans, M. Polanyi, *Trans. Faraday Soc.* **1936**, pp 1333–1360.

[53] E. T. McBee, C. G. Hsu, O. R. Pierce, C. W. Roberts, *J. Am. Chem. Soc.* **1955**, *77*, 915–917.

[54] M. Essers, C. Mück-Lichtenfeld, G. Haufe, *J. Org. Chem.* **2002**, *67*, 4715–4721.

[55] L. Merzoud, A. Saal, R. Moussaoui, O. Ouamerali, C. Morell, H. Chermette, *Phys. Chem. Chem. Phys.* **2018**, *20*, 16102–16116.

[56] K. Shibatomi, K. Futatsugi, F. Kobayashi, S. Iwasa, H. Yamamoto, *J. Am. Chem. Soc.* **2010**, *132*, 5625–5627.

[57] A. M. Sarotti, R. A. Spanevello, A. G. Suárez, *Tetrahedron Lett.* **2011**, *52*, 4145–4148.

[58] J. Sauer, H. Wiest, A. Mielert, *Chem. Ber.* **1964**, *97*, 3183–3207.

[59] K. N. Houk, R. J. Loncharich, J. F. Blake, W. L. Jorgensen, *J. Am. Chem. Soc.* **1989**, *111*, 9172–9176.

[60] D. Yepes, O. Donoso-Tauda, P. Pérez, J. S. Murray, P. Politzer, P. Jaque, *Phys. Chem. Chem. Phys.* **2013**, *15*, 7311–7320.

[61] M. J. S. Dewar, J. J. P. Stewart, S. Olivella, *J. Am. Chem. Soc.* **1986**, *108*, 5771–5779.

[62] P. Brown, R. C. Cookson, *Tetrahedron* **1965**, *21*, 1993–1998..

[63] B. J. Levandowski, T. A. Hamlin, F. M. Bickelhaupt, K. N. Houk, *J. Org. Chem.* **2017**, *82*, 8668–8675.

[64] E. J. Corey, *Angew. Chem. Int. Ed.* **2002**, *41*, 1650–1667; *Angew. Chem.* **2002**, *114*, 1724–1741.

[65] T. Salavati-Fard, S. Caratzoulas, D. J. Doren, *J. Phys. Chem. A* **2015**, *119*, 9834–9843.